Title

Quantitative Brightness Analysis of Protein Oligomerization in the Nuclear Envelope.

Journal

Biophysical Journal, 113(1)

Authors

Hennen, Jared
Hur, Kwang-Ho
Saunders, Cosmo
et al.

Publication Date

2017-07-11

DOI

10.1016/j.bpj.2017.05.044

Peer reviewed

Biophysical Journal
Article

Biophysical Society

Quantitative Brightness Analysis of Protein Oligomerization in the Nuclear Envelope

Jared Hennen,[1] Kwang-Ho Hur,[1] Cosmo A. Saunders,[2] G. W. Gant Luxton,[2] and Joachim D. Mueller[1,3,*]
[1]School of Physics and Astronomy, [2]Department of Genetics, Cell Biology, and Development, and [3]Department of Biomedical Engineering, University of Minnesota, Minneapolis, Minnesota

ABSTRACT Brightness analysis of fluorescence fluctuation experiments has been used to successfully measure the oligomeric state of proteins at the plasma membrane, in the nucleoplasm, and in the cytoplasm of living cells. Here we extend brightness analysis to the nuclear envelope (NE), a double membrane barrier separating the cytoplasm from the nucleoplasm. Results obtained by applying conventional brightness analysis to fluorescently tagged proteins within the NE exhibited an unusual concentration dependence. Similarly, the autocorrelation function of the fluorescence fluctuations exhibited unexpected changes with protein concentration. These observations motivated the application of mean-segmented Q analysis, which identified the existence of a fluctuation process distinct from molecular diffusion in the NE. We propose that small changes in the separation of the inner and outer nuclear membrane are responsible for the additional fluctuation process, as suggested by results obtained for luminal and nuclear membrane-associated EGFP-tagged proteins. Finally, we applied these insights to study the oligomerization of the luminal domains of two nuclear membrane proteins, nesprin-2 and SUN2, which interact translumenally to form a nuclear envelope-spanning linker molecular bridge known as the linker of the nucleoskeleton and cytoskeleton complex.

INTRODUCTION

The nuclear envelope (NE) (Fig. 1 *A*) surrounds the nucleus and consists of the inner nuclear membrane (INM) and outer nuclear membrane (ONM). Both membranes are separated by a thin (~30–50 nm) lumen or perinuclear space (PNS) (1). This structure limits the free diffusion of molecules between the cytoplasm and the interior of the nucleus whereas nuclear pore complexes within the NE regulate transport between these two compartments (2). In addition to its well-known function as a physical barrier, it has become increasingly clear that important chemical and mechanical signaling events are coordinated by proteins in the NE (3,4). Its vital role within the cell is further demonstrated by recent research showing an association between mutations in genes encoding NE proteins and several human diseases, including DYT1 dystonia, muscular dystrophy, cancer, and many other laminopathies (3,5). However, the majority of NE proteins are poorly characterized, which in part reflects the lack of tools capable of quantifying protein-protein interactions within this subcellular compartment.

To address this shortcoming, this study explores the potential of fluorescence fluctuation spectroscopy (FFS) for characterizing protein behavior in the NE. FFS is routinely used to measure the mobility and concentration of proteins as well as the average photon count rate per labeled protein complex, a property known as "brightness" (6,7). The normalized brightness b, which is defined as the ratio of the measured brightness to the brightness of the label EGFP, provides a direct readout of the average oligomeric state of the labeled protein (8,9). E.g., a monomeric protein corresponds to a brightness of $b = 1$, whereas dimerization of the monomer doubles the brightness to $b = 2$. This concept has been successfully employed to study protein oligomerization in the cytoplasm, nucleoplasm, and plasma membrane of mammalian cells (10–12).

Here, we demonstrate that conventional analysis of FFS data taken in the NE leads to perplexing results, prompting the use of the recently described mean-segmented Q (MSQ) analysis method (13). MSQ identified the existence of an additional fluctuation process linked to the subcellular environment of the NE. After characterizing this fluctuation process, we applied MSQ to investigate the oligomeric state of the luminal domains of the INM Sad1/UNC-84 (SUN) protein SUN2 and the ONM protein nesprin-2, the luminal domains of which interact within the PNS to form the core of

Submitted April 7, 2017, and accepted for publication May 30, 2017.
*Correspondence: mueller@physics.umn.edu
Editor: David Piston.
http://dx.doi.org/10.1016/j.bpj.2017.05.044

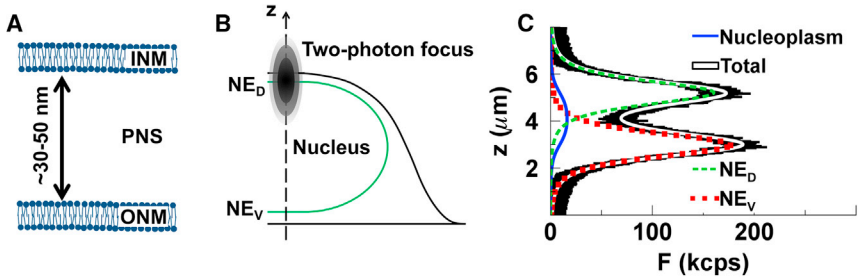

FIGURE 1 Z-scan through the NE. (*A*) Shown here is a schematic of the NE with the perinuclear space (PNS) surrounded by an inner and outer nuclear membrane. (*B*) Given here is an illustration of a z-scan through a cell expressing a fluorescent protein in the NE (*green line*). (*C*) Given here is a Z-scan intensity profile (*black line*) for SS-EGFP with a fit to a $\delta s\delta$-model showing the intensity contributions from the NE_V and NE_D as well as the nucleoplasmic contribution. To see this figure in color, go online.

the linker of cytoskeleton and nucleoskeleton complex (14). This NE-spanning molecular bridge is responsible for the mechanical integration of the nucleus with the rest of the cell, which is required for several fundamental cellular functions including DNA damage repair, meiotic chromosome pairing, nuclear positioning, and the mechanoregulation of gene expression (15–17). Recently published in vitro studies show that the luminal domain of SUN2 homotrimerizes to form binding sites for the luminal Klarsicht/ANC-1/SYNE homology (KASH) peptide of nesprin-2 between adjacent SUN2 monomers (18). We tested this model by measuring SUN2 oligomerization in the NE and demonstrate that live-cell FFS provides a promising approach for studying NE proteins in their native environment.

MATERIALS AND METHODS

Experimental setup

Experiments were performed with an excitation wavelength of 1000 nm and an average power after the objective of 0.3–0.4 mW on a two-photon microscope with a 63× C-Apochromat water immersion objective with numerical aperture (NA) = 1.2 (Zeiss, Oberkochen, Germany) as described in Smith et al. (12,19). A few select measurements were performed with a 20× Plan-Apochromat immersionless objective (NA = 0.8; Zeiss). Photon counts were detected by an avalanche photodiode (SPCM-AQ-141 APD; PerkinElmer, Dumberry, Quebec, Canada), recorded by a Flex04-12D card (correlator.com, Bridgewater, NJ) with a sampling frequency of 20 kHz, and analyzed with programs written in IDL 8.5 (Research Systems, Boulder, CO). All z-scans were performed using an arbitrary waveform generator (model No. 33522A; Agilent Technologies, Santa Clara, CA) to move a PZ2000 piezo stage (ASI, Eugene, OR) axially. The driving signal from the arbitrary waveform generator was a linear ramp function with a peak-to-peak amplitude of 1.6 V and a period of 10 s. The peak-to-peak voltage corresponded to 24.1 μm of axial travel at a speed of v_z 4.82 μm/s.

Sample preparation

All experiments were conducted using transiently transfected U2OS cells obtained from ATCC (Manassas, VA) and maintained in DMEM with 10% fetal bovine serum (Hyclone Laboratories, Logan, UT). Cells were subcultured into 24-well glass bottom plates (In Vitro Scientific, Sunnyvale, CA) before transfection. GenJet (SignaGen Laboratories, Rockville, MD) was used to transiently transfect cells 12–24 h before measurement, according to the manufacturer's instructions. The growth medium was replaced with Dulbecco's phosphate-buffered saline containing calcium and magnesium (BioWhittaker, Walkerville, MD) immediately before measuring. Information regarding the construction of the cDNA constructs used in this work is described in the Supporting Material.

Z-scan analysis

A modified squared Gaussian-Lorentzian point spread function (PSF) was used to analyze z-scan FFS data (20). Z-scan calibration was performed as described in MacDonald et al. (20) to determine the radial and axial beam-waist (ω_0 and z_0) as well as the axial decay parameter y, resulting in values of $\omega_0 = 0.45 \pm 0.05$ μm, $z_0 = 1.0 \pm 0.1$ μm, and $y = 2.4 \pm 0.3$ μm. The z-scan intensity profile $F(z)$ was fit by the $\delta s\delta$-model (12) to identify the intensity contributions from the ventral NE (NE_V) at height z_V, the dorsal NE (NE_D) at height z_D, and the nuclear layer in between, $F(z) = F_V(z, z_V) + F_N(z, z_V, z_D) + F_D(z, z_D)$. Because the NE is much thinner than the axial size of the PSF, it is modeled by an infinitesimally thin layer, which we refer to as a δ-layer, whereas the nucleoplasm is modeled by a slab or s-layer (20). The intensity $F(z_V)$ represents the signal with the focus of the PSF on the NE_V, whereas $f_V = F_V(z_V, z_V)/F(z_V)$ describes the fraction of the fluorescence intensity from the NE_V at this location. The corresponding intensity fraction f_D from the NE_D is defined analogously.

FFS analysis

The fluorescence fluctuation data were analyzed using the following methods. Q-analysis (21,22) was applied to determine Mandel's Q value after accounting for dead time and afterpulsing effects. Brightness λ was determined from Q and the sampling time Δt by the relation $Q = \gamma_2\lambda\Delta t$. The second-order shape factor γ_2 was determined from analysis of the z-scan intensity profile (12,20). Control experiments were conducted to determine the brightness λ_{EGFP} of the fluorescent label EGFP (23). The normalized brightness, $b = \lambda/\lambda_{EGFP}$, characterizes the average oligomeric state of the EGFP-tagged proteins (20), i.e., a monomer leads to $b = 1$, whereas a dimer results in $b = 2$, and a mixture would produce a b between 1 and 2. To plot b binding curves, an indicator of protein concentration is needed. We used the average number of monomers residing in our PSF, which was calculated as $N = \langle F\rangle/\lambda_{EGFP}$ with F representing the fluorescence intensity expressed as photon counts per second. The parameter N can also be interpreted as a number density per unit volume V_0.

The autocorrelation function (ACF) of the fluorescence intensity was calculated and fit to a model of 2D diffusion, as follows:

$$G(\tau) = \frac{G(0)}{1 + \tau/\tau_d}, \tag{1}$$

with fluctuation amplitude $G(0)$, lag time τ, and diffusion time τ_d. Some ACF data were fit adding an exponential correlation term, as follows:

$$G(\tau) = \frac{A_0}{\langle F\rangle\Delta t}\exp(-\tau/T_0), \tag{2}$$

with characteristic decay time T_0 and amplitude factor A_0 to Eq. 1.

MSQ divides the FFS data into segments of duration T and determines the Q value averaged over all segments, MSQ(T). The model describing MSQ for a single diffusing species is as follows (13):

$$\mathrm{MSQ}_{\mathrm{diff}}(T) = Q\left(1 - \frac{B_2(T,\tau_d)}{T^2}\right) - \frac{\Delta t}{T}, \quad (3)$$

where $B_2(T,\tau_d)$ is the second-order binning function (24,25). Fitting the MSQ data to this model determines Mandel's Q and the diffusion time τ_d. The MSQ of two diffusing species is given by the following:

$$\mathrm{MSQ}_{\mathrm{diff,2species}}(T) = f_1\mathrm{MSQ}_{\mathrm{diff}}(Q_1,\tau_{d1},T) + f_2\mathrm{MSQ}_{\mathrm{diff}}(Q_2,\tau_{d2},T), \quad (4)$$

where f_1 and f_2 are the fractional intensities with $f_2 = 1 - f_1$. The amplitudes of each process, Q_1f_1 and Q_2f_2, of Eq. 4 are related to the effective normalized brightness b of the MSQ curve as follows,

$$\frac{Q_1f_1}{Q_2f_2} = \frac{b_1(b-b_2)}{b_2(b_1-b)}, \quad (5)$$

where b_i is the normalized brightness of the ith component, and is derived utilizing the relations $b = b_1f_1 + b_2f_2$ and $Q_1/Q_2 = b_1/b_2$.

Experimental protocol

After selecting a fluorescent cell by epifluorescence microscopy, FFS data was acquired by first taking a z-scan through the nucleus followed by focusing the two-photon beam on the NE_V to collect intensity fluctuations for ~60 s. Next, the beam was focused on the NE_D to acquire intensity fluctuations followed by an additional z-scan. Because FFS analysis assumes a stationary process (26), any fluctuation data with sudden intensity jumps or slow drifts in the intensity were rejected. Comparison of the initial and final z-scan intensity profile served to identify mechanical drift of the stage or cell motion that occurred during the FFS measurement process. Measurements where the initial and final z-scan intensity profile differed were discarded. The z-scan FFS data were analyzed as described above.

RESULTS AND DISCUSSION

Z-scan FFS and conventional analysis of EGFP within the NE

EGFP has been successfully used as a brightness marker of protein oligomerization in the cytoplasm, nucleoplasm, and at the plasma membrane of living cells (13–15). Because the NE was, to our knowledge, a new environment for brightness studies, we needed to establish the suitability of EGFP as a quantitative brightness marker in this subcellular compartment. We targeted EGFP to the contiguous lumen of the ER and the NE by fusing the signal sequence (SS) of the luminal protein torsinA to the N-terminus of EGFP (27). Expression of SS-EGFP in U2OS cells resulted in its efficient localization to the NE as corroborated by z-scan intensity profiles taken through the nucleus (Fig. 1 *B*). A typical z-scan intensity profile from a SS-EGFP-expressing cell displayed two prominent peaks corresponding to fluorescence emanating from the NE_V and NE_D (Fig. 1 *C*). $F(z)$ was fit to a three-layer $\delta s \delta$ model consisting of a thick nucleoplasmic layer separating two thin NE layers. The fit demonstrated that the NE layers were the main sources of fluorescence in this SS-EGFP-expressing cell (Fig. 1 *C*). The intensity fraction values originating at the NE_V and NE_D for this intensity profile were 94 and 93%, respectively. For the remainder of this work, only cells with NE intensity fractions >90% were used for FFS measurements. This criterion significantly simplifies data analysis, as it ensures that non-NE fluorescence contributions are sufficiently small to be ignored (12).

FFS measurements with the two-photon focus at either the NE_V or NE_D of SS-EGFP-expressing cells were used to determine the normalized brightness b of SS-EGFP in the NE using conventional brightness analysis (20,21). We observed an unexpected increase of b for SS-EGFP from ~1 to 2 with number concentration N (Fig. 2 *A*). Repeating the experiment with a tandem-dimeric $EGFP_2$ (23) fused behind the torsinA SS ($SS\text{-}EGFP_2$) resulted in a similar increase of b with N from 2 to values exceeding 3 (Fig. 2 *A*). In contrast, brightness measurements of EGFP and $EGFP_2$ in the cytoplasm resulted in stable b values of 1 and 2, as expected for a monomeric and dimeric protein (Fig. 2 *B*). The N-dependent increase in b was also observed for SS-tagged mTurquoise (SS-mTurquoise) and enhanced yellow fluorescent protein (SS-EYFP) in the NE, indicating that this behavior was not specific to EGFP (Fig. 2 *C*). Moreover, we observed that the decay shape of the ACF for SS-EGFP exhibited a pronounced broadening with N (Fig. 2, *D* and *E*). In particular, the single-species diffusion model (Eq. 1) agreed well with data measured at low N values, but no longer accurately described the data measured as N increased.

MSQ analysis of FFS experiments performed in the NE

Because established FFS analysis methods yielded perplexing results, we turned to MSQ, which has proved useful to characterize fluctuations caused by diffusion in the presence of additional slow variations of the fluorescence signal (13). MSQ first divides the FFS intensity trace into segments of period T (Fig. 3 *A*, *top*), then calculates the local Q value of each segment, which are then averaged together to determine MSQ(T). This process is repeated for a range of segment times T (Fig. 3 *A*, *bottom*). Measurement of cytoplasmic EGFP resulted in an MSQ curve that initially increased with T and then plateaued (Fig. 3 *B*). The value of MSQ(T) reflects the average Q taken over T, which only accounts for fluctuations with a correlation time less than T (13). Thus, the initial increase in the MSQ value with T reflects the inclusion of longer timescale dynamics. Once T is large enough that fluctuations with the longest correlation time are sampled, the MSQ value plateaus. Fitting the MSQ curve to the single-species diffusion model

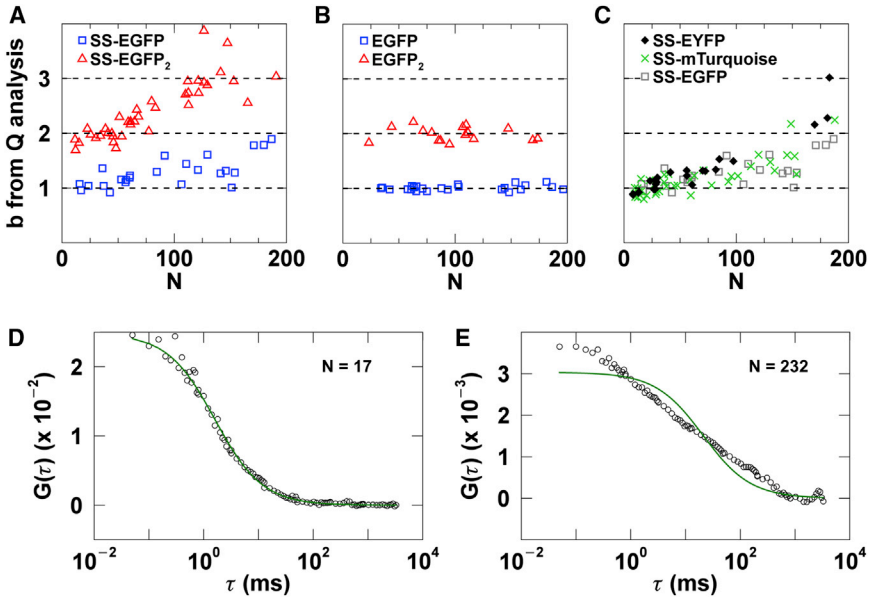

FIGURE 2 Conventional analysis of FFS data generated by fluorescent proteins in the NE or cytoplasm. (*A–C*) Given here is the brightness b from Q analysis versus number concentration N. (*A*) Shown here is SS-EGFP and SS-EGFP$_2$ in the NE. (*B*) Shown here is EGFP and EGFP$_2$ in the cytoplasm with mean values of $b = 1.01 \pm 0.05$ and $b = 1.99 \pm 0.1$, respectively. (*C*) Shown here is SS-EYFP, SS-mTurquoise, and SS-EGFP in the NE. (*D* and *E*) Given here is the ACF of SS-EGFP in the NE at different N values. ACFs were fit to a single-species diffusion model (*green line*). To see this figure in color, go online.

(Eq. 3) resulted in a diffusion time $\tau_d = 0.57 \pm 0.22$ ms and $Q = 0.016 \pm 0.001$, which corresponded to $b = 1.12$ (Fig. 3 *B*). These values were consistent with the results obtained from the ACF ($\tau_d = 0.68 \pm 0.04$ ms) and conventional brightness analysis ($b = 1.05$).

Note that our standard algorithms for calculating the ACF and brightness are also performed on segmented data using a predetermined T, because this approach improves the robustness of FFS analysis of cellular data (28). We typically use a segment time of 6.5 s, which is within the plateau region of the MSQ curve generated for EGFP in the cytoplasm (Fig. 3 *B*), and therefore accounts for all correlated fluctuations. Under these conditions, we expect that MSQ and traditional FFS analysis would lead to similar results, as experimentally verified above.

To determine if MSQ analysis can be used for b measurements in thin cell layers, we next measured the EGFP-tagged peripheral membrane protein HRas (HRas-EGFP) at the plasma membrane (16). The MSQ curve for HRas-EGFP also featured a plateau region, although at larger T than observed for EGFP in the cytoplasm (Fig. 3, *B* and *C*). This result reflects the lower mobility of HRas-EGFP, which leads to a longer persistence of correlated fluctuations due to diffusion. A fit to the single-species diffusion model (Eq. 3) was sufficient to describe the MSQ of HRas-EGFP (Fig. 3 *C*). After accounting for the γ-factor of a thin layer (20), the fitted Q value corresponded to $b = 0.99$. This value indicated that HRas-EGFP was monomeric, consistent with our previously reported result based on conventional brightness analysis (12). This agreement was expected, as the segment time of 6.5 s is within the plateau region of the MSQ curve (Fig. 3 *C*).

The results described above demonstrate that MSQ reliably identifies the brightness of proteins within thick and thin sample layers. However, the MSQ of SS-EGFP within the NE produced a curve without a clearly identifiable plateau region and could not be described by the single-species diffusion model (*solid green line*, Fig. 3 *D*). The absence of a plateau region indicates that conventional FFS analysis is no longer applicable as some fluctuations persist longer than the segment time. We found empirically that adding an additional process with an MSQ term of

$$\mathrm{MSQ}_{\mathrm{exp}}(T, T_0) = A_0\left(1 - \frac{\mathrm{B}_{2,\mathrm{exp}}(T/T_0)}{(T/T_0)^2}\right) \qquad (6)$$

resulted in good agreement with the MSQ curve obtained for SS-EGFP in the NE (*dashed red line*, Fig. 3 *D*). Equation 6 represents the MSQ of an exponential correlation process (Eq. 2) with amplitude A_0, decay time T_0, and the following binning function:

$$B_{2,\mathrm{exp}}(x) = 2\left(x + e^{-x} - 1\right). \qquad (7)$$

Equations 6 and 7 were derived following the procedure described by Hur and Mueller (13).

To test whether the combination of a diffusion and exponential correlation process described the intensity fluctuations of SS-EGFP in the NE, we applied this model to all SS-EGFP data by fitting each experimental MSQ curve to the sum of Eqs. 3 and 4. The fitted Q and τ_d values from the diffusion process stayed approximately constant at low ($N = 16$, $Q = 0.022 \pm 0.001$, and $\tau_d = 1.2 \pm 0.3$ ms) and high ($N = 91$, $Q = 0.023 \pm 0.001$, and $\tau_d = 1.4 \pm 0.4$ ms) N values (Fig. 4, *A* and *B*). Converting all fitted Q values to b revealed that SS-EGFP is monomeric ($b = 1.06 \pm 0.14$) at all measured N (Fig. 4 *C*). Similarly,

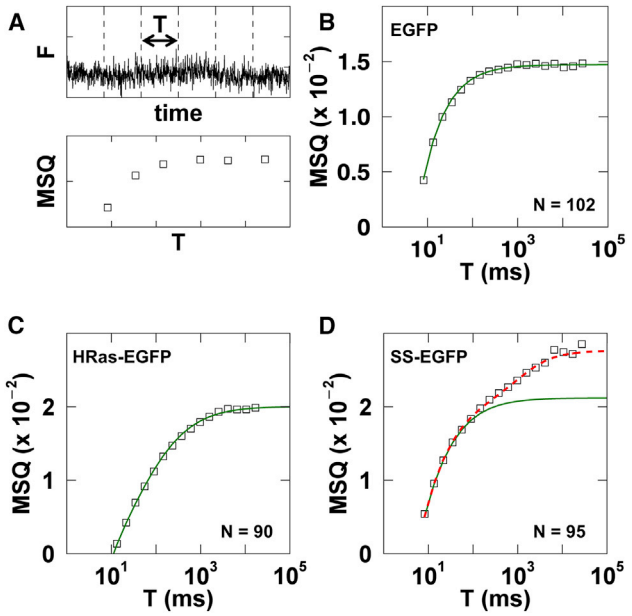

FIGURE 3 MSQ analysis of FFS data taken in the cytoplasm, at the plasma membrane, and in the NE. (*A*) Given here is an illustration of MSQ calculation. (*Top*) Segmentation of FFS data into T; (*bottom*) plot of MSQ data versus T. (*B* and *C*) Given here is the MSQ (*squares*) versus segment time with fit to a single diffusion model (*solid green line*). (*B*) Given here is EGFP in the cytoplasm with fitted $Q = 0.016 \pm 0.001$ (corresponding to $b = 1.05$) and $\tau_d = 0.57 \pm 0.22$ ms. (*C*) Given here is HRas-EGFP at the plasma membrane with fitted $Q = 0.021 \pm 0.003$ (corresponding to $b = 0.99$) and $\tau_d = 16 \pm 1$ ms. (*D*) Shown here is the MSQ (*squares*) versus segment time from SS-EGFP in the NE. (*Dashed red line*) Here is the fit to a diffusion model plus exponential correlation process with fitted $Q = 0.026 \pm 0.004$ (corresponding to $b = 1.13$) and $\tau_d = 1.7 \pm 0.3$ ms. (*Solid green line*) The diffusion component of the fit is shown. To see this figure in color, go online.

we found that the brightness of SS-EGFP$_2$ in the NE was N-independent with a mean value of $b = 1.97 \pm 0.19$, consistent with a dimeric protein.

However, a strong difference in A_0 was observed when the MSQ data of SS-EGFP in the NE with low and high N values were compared (Fig. 4, *A* and *B*). The fitted A_0 of SS-EGFP and SS-EGFP$_2$ increased approximately proportionally with intensity as demonstrated by a linear regression through the origin with a slope of 1.0×10^{-4} kHz^{-1} (*green line*, Fig. 4 *D*). The diffusion time τ_d of all fitted values for SS-EGFP in the NE was N-independent with a mean and standard deviation (SD) of 2.4 ± 1 ms (*dashed blue line*, Fig. 4 *E*). Similarly, the τ_d measured for SS-EGFP$_2$ was also independent of N with a mean and SD of 4.3 ± 2 ms (*dashed red line*, Fig. 4 *E*). Finally, the decay time T_0 of the exponential correlation process appeared to be N-independent with a mean of 1.7 ± 1.3 s (Fig. 4 *F*).

The MSQ analysis of FFS data taken for SS-EGFP and SS-EGFP$_2$ in the NE supported a model where intensity fluctuations are caused by a combination of diffusion and a process with an exponential correlation term. Because we suspected that the unusual shape of the ACF (Fig. 2 *E*) was a direct consequence of this additional process, we tested for agreement between MSQ and ACF analysis. Fitting the MSQ curve identified four parameters, Q, τ_d, A_0, and T_0. These parameters served to calculate the predicted ACF curve using the equation:

$$G(\tau) = \frac{Q}{\langle F\rangle \Delta t}\frac{1}{1+\tau/\tau_d} + \frac{A_0}{\langle F\rangle \Delta t}\exp\left(-\frac{\tau}{T_0}\right), \qquad (8)$$

where $Q/(\langle F\rangle \Delta t)$ corresponds to the fluctuation amplitude $G(0)$ of the diffusion process from Eq. 1, and the second term represents the exponential correlation. However, this approach failed to reproduce the experimental ACF for FFS data collected for SS-EGFP in the NE (Fig. 5). Although the MSQ fit was in good agreement with the MSQ data (Fig. 5 *A*), the calculated ACF curve deviated significantly from the experimental ACF (*dashed red line*, Fig. 5 *B*). In particular, our model (Eq. 8) overestimated the amplitude of the exponential correlation process in the ACF.

We determined that this discrepancy stemmed from the finite segment time ($T = 6.5$ s) used in calculating the ACF, which was too short to sample all correlated fluctuations of the exponential correlation process. Therefore, we modified the previous equation using the theoretical approach described by Hur and Mueller (13) to include the effect of the finite segment time, as follows:

$$G(\tau) = \frac{Q}{\langle F\rangle \Delta t}\frac{1}{1+\frac{\tau}{\tau_d}} + \frac{A_0}{\langle F\rangle \Delta t}\left(e^{-\frac{\tau}{T_0}} - \frac{B_{2,\exp}(T/T_0) + B_{2,\exp}(|T-2\tau|/T_0) - 2B_{2,\exp}(\tau/T_0)}{2\left(\frac{T-\tau}{T_0}\right)^2}\right). \qquad (9)$$

The second term reflects the estimator bias for an exponential correlation e^{-t/T_0}, which leads to binning functions (25) as described in Hur et al. (26). The application of Eq. 9 rather than Eq. 8 to predict the ACF led to a good agreement between data and model (*solid red line*, Fig. 5 *B*).

Origin of the exponential correlation process

To test whether the exponential correlation process is caused by intensity fluctuations of individual SS-EGFP proteins or

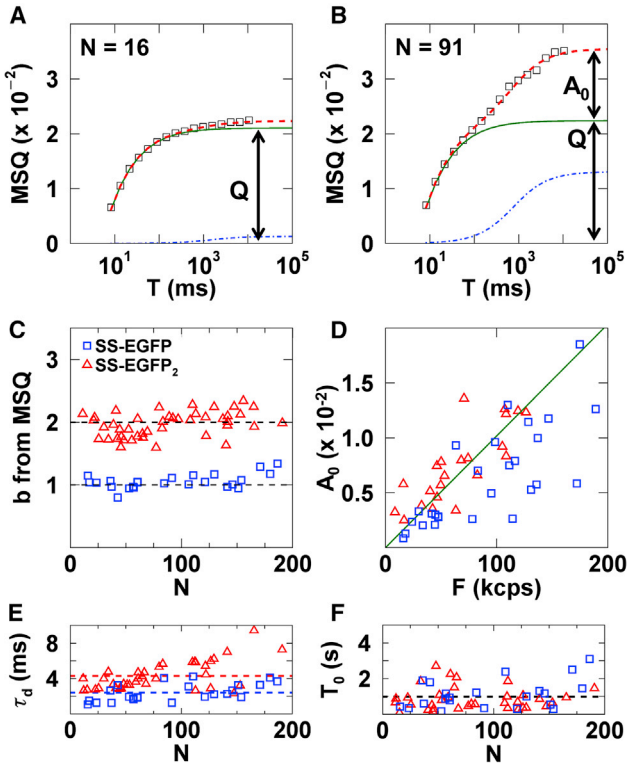

FIGURE 4 MSQ analysis of FFS data from SS-EGFP and SS-EGFP$_2$ in the NE. (*A* and *B*) Shown here is MSQ (*squares*) versus segment time for SS-EGFP at different *N* values. (*Dashed red line*) Given here is the fit to a single diffusion plus exponential correlation model; (*solid green line*) diffusion component; (*dot-dashed blue line*) exponential correlation component. (*C*) Given here is a plot of *b* versus *N* for SS-EGFP and SS-EGFP$_2$ calculated from MSQ analysis. (*D*) Given here is a plot of A_0 versus mean fluorescence intensity with a linear fit (*solid green line*). (*E*) Given here is a plot of τ_D versus *N*; (*dashed lines*) mean value. (*F*) Given here is a plot of T_0 versus *N*; (*dashed line*) mean value. (*C–F*) Data from SS-EGFP and SS-EGFP$_2$ are plotted (*blue squares* and *red triangles*, respectively). To see this figure in color, go online.

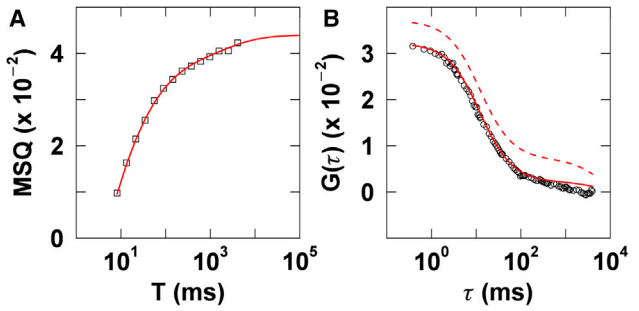

FIGURE 5 Comparison between MSQ and ACF for SS-EGFP in the NE. (*A*) Given here is the MSQ (*squares*) versus *T* for SS-EGFP with a fit to the diffusion plus exponential correlation model (*red line*). (*B*) Given here is an experimental ACF (*circles*) calculated with a segment time $T = 6.5$ s. Predicted ACF curves are based on fitted MSQ parameters using Eq. 8 (*dashed red line*) and Eq. 9 (*solid red line*). To see this figure in color, go online.

by a collective process, we measured the ACF for SS-EGFP in the NE using first a water immersion objective with high NA and then an immersionless objective with lower NA (Fig. 6). The ACFs were fit to Eq. 9 (*dashed red line*, Fig. 6) with the diffusion term (*solid green line*) and the exponential correlation term (*dot-dashed blue line*) shown for comparison. These fits provide insight into the effect of NA on two sets of parameters, the temporal parameters τ_d and T_0, and the amplitude parameters Q and A_0. The diffusion time τ_d for SS-EGFP in the NE increased from 1.5 ms for the high to 4.6 ms for the low NA objective, reflecting the larger radial beam waist of the latter. On the other hand, T_0 was reduced by a factor of ~2 ($T_{0\text{water}} = 1.6$ s, $T_{0\text{air}} = 0.7$ s). This approximately sevenfold difference between the change seen in τ_d and T_0 implies that this process is not diffusive.

The fitted Q value changed by a factor of ~30 after the switch from the high ($Q_{\text{water}} = 0.02$) to the low ($Q_{\text{air}} = 0.0007$) NA objective. Because Q represents a single molecule property, which is independent of concentration or volume, the decrease reflects the change in excitation intensity and collection efficiency between both objectives. If A_0 were to represent a molecular property, then we would expect to observe a corresponding 30-fold reduction in amplitude upon switching objectives. However, A_0 only changed by a factor of 2 ($A_{0\text{water}} = 0.0025$, $A_{0\text{air}} = 0.0012$), which indicates that this process is not related to intensity fluctuations of individual molecules. Collective phenomena, on the other hand, are expected to lead to intensity fluctuations that scale with the observed volume, which provides a potential explanation why the amplitude A_0 reduced much less than 30-fold.

Thus, we investigated whether the exponential correlation process is consistent with the presence of local volume fluctuations of the NE. Fluctuations in the relative position of the INM and ONM would change the distance *h* separating these membranes, altering the luminal volume enclosed between both membranes (Fig. 7 *A*). Fluctuations in *h*, volume,

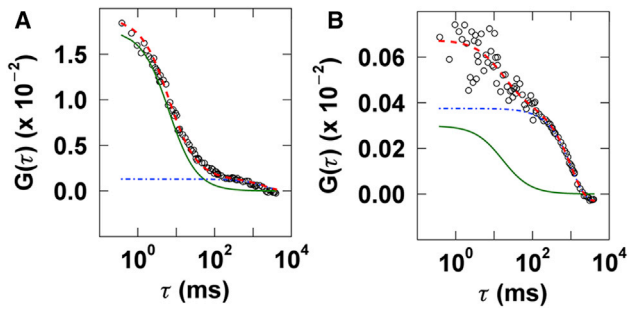

FIGURE 6 ACF of SS-EGFP in the NE taken with a high and a low NA objective. Here, ACF is taken with a high NA water immersion objective (*A*) and a low NA immersionless objective (*B*). Both experimental ACF curves (*circles*) were fit to Eq. 9 (*dashed red line*). The fitted diffusion (*solid green line*) and exponential (*dot-dashed blue line*) components are shown for comparison. To see this figure in color, go online.

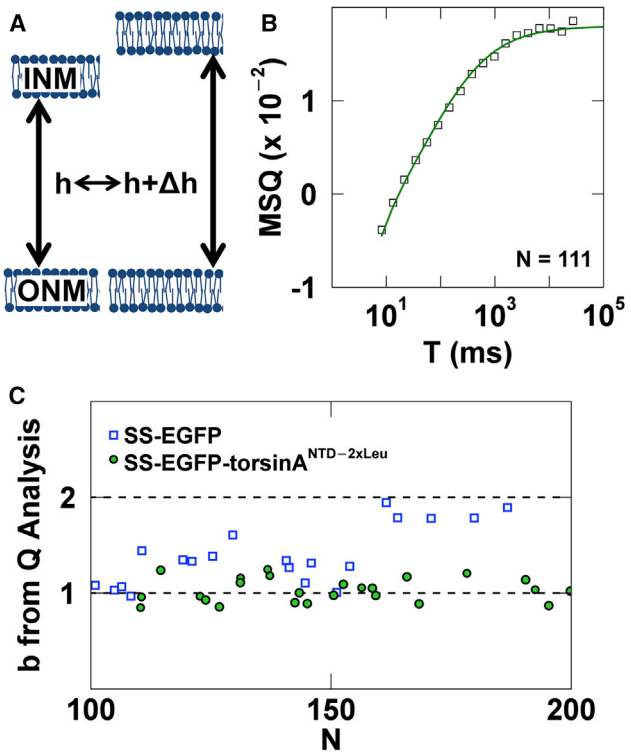

FIGURE 7 Distance fluctuations between the INM and ONM. (*A*) Illustration of fluctuations in the distance h separating the two nuclear membranes is given. (*B*) Shown here is an MSQ curve (*squares*) for SS-EGFP-torsinA$^{NTD-2xLeu}$ in the NE fit to a single-species diffusion model (*green line*). (*C*) Given here is a plot of b from conventional brightness analysis versus N for SS-EGFP and SS-EGFP-torsinA$^{NTD-2xLeu}$ in the NE. To see this figure in color, go online.

and fluorescence intensity all would have the same relative SD, as follows:

$$\sqrt{\langle \Delta h^2 \rangle} \Big/ \langle h \rangle = \sqrt{\langle \Delta V^2 \rangle} \Big/ \langle V \rangle = \sqrt{\langle \Delta F^2 \rangle} \Big/ \langle F \rangle = c. \tag{10}$$

We further anticipate that the fluctuations in h are a property intrinsic to the NE and therefore independent of the expressed protein concentration, which implies that the variance $\langle \Delta h^2 \rangle$ is approximately constant. As a consequence, the relative SD $\sqrt{\langle \Delta h^2 \rangle}/\langle h \rangle$ of Eq. 10 has to be equal to a constant value c. Furthermore, the A_0 value of the volume fluctuations is determined by $A_0 = \langle \Delta F^2 \rangle / \langle F \rangle \Delta t$, which can be rewritten using Eq. 10, as follows:

$$A_0 = c^2 \Delta t \langle F \rangle. \tag{11}$$

This equation predicts that A_0 is directly proportional to the fluorescence intensity $\langle F \rangle$ as was experimentally observed (Fig. 4 *D*). Equation 11 was applied to determine that $c = 0.06$ from the fitted slope of Fig. 4 *D* and a sampling time $\Delta t = 50$ μs. Because c represents the relative SD of $\sqrt{\langle \Delta h^2 \rangle}/\langle h \rangle$, knowing the average distance $\langle h \rangle$ specifies the fluctuation amplitude $\sqrt{\langle \Delta h^2 \rangle}$. Assuming an average distance of 40 nm between the INM and the ONM, we predicted that subtle variations (~2 nm) in the axial distance between these membranes would be sufficient to give rise to the observed exponential correlation process. The equilibrium out-of-plane motion of a biomembrane in a viscous environment is described by an exponential decay of each spatial mode with its own characteristic time (29). Thus, the observation of an exponential correlation process indicates that the range of modes observed in our studies is very restricted. This is plausible due to the high density of NE-embedded nuclear pore complexes, which provide local restraints for the motion of the membranes.

We further predicted that FFS measurements of nuclear membrane-associated proteins would not be sensitive to these volume fluctuations, as axial motion by a few nanometers within the PSF is experimentally undetectable. To test this prediction, SS-EGFP was fused with a previously characterized transmembrane domain generated by two leucine substitutions within the hydrophobic membrane-associating N-terminal domain (NTD) of torsinA (SS-EGFP-torsinA$^{NTD-2xLeu}$) (30). The MSQ of FFS data collected for SS-EGFP-torsinA$^{NTD-2xLeu}$ in the NE with $N = 111$ resulted in a curve that plateaued at large T. The data were described by the single-species diffusion model with $Q = 0.018$ and $\tau_d = 26$ ms, which is consistent with the absence of the exponential correlation process observed for SS-EGFP in the NE (Fig. 7 *B*). Repeated measurements in the NE of SS-EGFP-torsinA$^{NTD-2xLeu}$ expressing cells resulted in a mean value of $\tau_d = 40 \pm 20$ ms, which was significantly slower than the value obtained for SS-EGFP in the same subcellular compartment ($\tau_d = 2.4 \pm 1.0$ ms), as expected for a membrane-bound protein.

Because the plateau region for the MSQ curve obtained for SS-EGFP-torsinA$^{NTD-2xLeu}$ in the NE includes $T = 6.5$ s, we were able to perform conventional brightness analysis. The b of SS-EGFP-torsinA$^{NTD-2xLeu}$ in the NE was monomeric ($b = 1.03 \pm 0.13$) and N-independent (Fig. 7 *C*), as opposed to the increase in b observed for SS-EGFP using the same conventional analysis (Fig. 2 *A*). This difference further supports the proposed model of nanometer-sized fluctuations in the axial distance between the INM and ONM.

Quantifying the oligomerization of physiologically relevant NE proteins

The results described above establish the suitability of EGFP as a quantitative brightness marker in the NE and the framework necessary for interpreting FFS data collected in this subcellular compartment. To test the applicability of this approach for the study of NE proteins, we investigated the oligomerization of nesprin-2 and SUN2. Because EGFP-tagged nesprin-2 and SUN2 constructs were previously shown to be immobile in the NE (31), we selected protein

domains that diffuse within the PNS for our initial FFS experiments. Specifically, we measured the oligomerization of the SS-EGFP-tagged KASH peptide of nesprin-2 (SS-EGFP-KASH2) and luminal domain of SUN2 (SS-EGFP-SUN2$^{261–731}$) in the NE.

Because the MSQ curves of SS-EGFP-KASH2 measured in the NE lacked a plateau region, the data was fit to the diffusion and exponential correlation model described above (Fig. 8 *A*). The fitted b values were N-independent with an average brightness of $b = 1.05 \pm 0.1$ (Fig. 8 *B*), indicating that SS-EGFP-KASH2 was monomeric in the NE. The diffusion time for SS-EGFP-KASH2 ($\tau_d = 4.0 \pm 1.4$ ms) in the NE was similar to the diffusion time observed for SS-EGFP$_2$ ($\tau_d = 4.3 \pm 1.6$ ms) in the same subcellular compartment (Fig. 4 *E*), suggesting that SS-EGFP-KASH2 diffuses through the PNS.

In contrast, FFS measurements taken in the NE of SS-EGFP-SUN2$^{261–731}$-expressing cells revealed features in the MSQ curve not shared by any of the other constructs previously measured in the NE. This is illustrated by the significant differences in the results of MSQ analysis for FFS data collected for SS-EGFP and SS-EGFP-SUN2$^{261–731}$ in the NE at $N = 14$ (Fig. 8 *C*). We deliberately chose FFS data with a low N to ensure that the influence of volume fluctuations on MSQ data is negligible. As expected, the MSQ curve for SS-EGFP was well characterized by the single-species diffusion model, confirming the absence of detectable PNS volume fluctuations, with a plateau value corresponding to a monomeric brightness. The maximum value of the MSQ curve of SS-EGFP-SUN2$^{261–731}$ significantly exceeded the maximum for SS-EGFP. Because the influence of volume fluctuations is negligible at this low concentration, the higher MSQ value corresponds to an increased brightness, indicating the presence of SS-EGFP-SUN2$^{261–731}$ oligomerization at $N = 14$. A single diffusion species was unable to reproduce the shape of the MSQ curve for SS-EGFP-SUN2$^{261–731}$. Increasing the number of diffusing species to two (Eq. 4) was sufficient to describe the experimental curve (*green line*, Fig. 8 *C*). The fit identified diffusion times of $\tau_{d1} = 8.5 \pm 0.2$ ms and $\tau_{d2} = 150 \pm 6$ ms. Comparison of these values with the diffusion time of the membrane-bound SS-EGFP-torsinA$^{NTD\text{-}2xLeu}$ (Fig. 7 *B*) revealed that τ_{d1} was too fast to represent a membrane-associated protein, whereas τ_{d2} was very slow and likely represents membrane-associated SS-EGFP-SUN2$^{261–731}$.

Fitting the experimental MSQ for SS-EGFP-SUN2$^{261–731}$ to Eq. 4 determined the total amplitude $Q = f_1Q_1 + f_2Q_2$, which was converted into a brightness b. This b increased in an N-dependent manner from ~1 to 3 (Fig. 8 *D*), which is consistent with a model of trimerization of SS-EGFP-SUN2$^{261–731}$. The fit also identified the diffusion times of the two components. Plotting τ_d versus N for SS-EGFP-SUN2$^{261–731}$ revealed that the fast and slow diffusion times were approximately N-independent (Fig. 8 *E*). The larger scatter in the fast diffusion times is likely caused by the lower MSQ amplitude of this component as compared to the slow process.

Protein trimerization involves a concentration-dependent mixture of monomers, dimers, and trimers. Because a two-species fit was sufficient to describe the experimental MSQ, the proportions of these oligomeric states cannot be determined. In fact, the two-species fit only determines the amplitudes f_1Q_1 and f_2Q_2, which are insufficient to determine the individual b values associated with Q_1 and Q_2. Interestingly, the ratio f_1Q_1/f_2Q_2, which indicates the relative contribution of the fast and slow population to the MSQ curve, decreased with increasing b (Fig. 8 *F*). This suggests that the amplitude of the fast diffusing species decreases relative

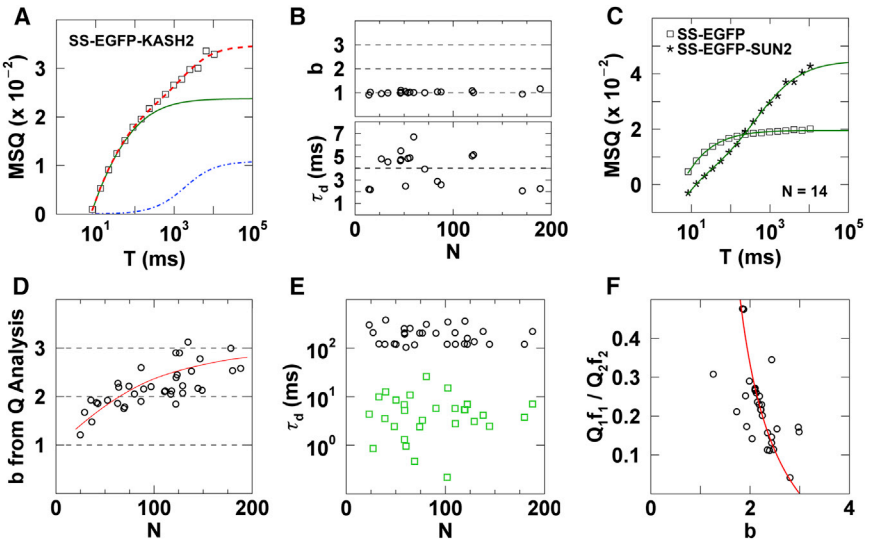

FIGURE 8 Measuring the oligomerization of SS-EGFP-KASH2 and SS-EGFP-SUN2$^{261–731}$ in the NE. (*A*) Given here is MSQ data for SS-EGFP-KASH2 fit to a diffusion plus exponential correlation model (*dashed red line*) with separated diffusion (*dot-dashed blue line*) and exponential correlation (*solid green line*) components. (*B*) Given here is a plot of b versus N (*top*) and τ_d versus N (*bottom*) for SS-EGFP-KASH2. (*C*) Given here is MSQ data for SS-EGFP (*squares*) and SS-EGFP-SUN2$^{261–731}$ (*stars*) at $N = 14$ with SS-EGFP fit to a single-species diffusion model (*green line*) and SS-EGFP-SUN2$^{261–731}$ fit to a two-species diffusion model (*green line*). (*D*) Given here is a plot of b from conventional Q analysis versus N for SS-EGFP-SUN2$^{261–731}$ with a red line added to guide the eye. (*E*) Given here is a plot of τ_d versus N for SS-EGFP-SUN2$^{261–731}$ showing the fast (*green squares*) and slow (*black circles*) components with an average of 5.8 and 190 ms, respectively. (*F*) Given here is a plot of ratio f_1Q_1/f_2Q_2 of the fast to slow diffusing species versus b of SS-EGFP-SUN2$^{261–731}$, with the red line representing the predicted relation for a monomer-trimer model. To see this figure in color, go online.

to the slow diffusing species as the average oligomerization of SS-EGFP-SUN2$^{261–731}$ increases.

Equation 5 establishes a relation between f_1Q_1/f_2Q_2 and b. A simple model assuming a monomer/trimer transition ($b_1 = 1$ and $b_2 = 3$) with the monomer and trimer representing the fast and slow components, respectively, agreed with the data (Fig. 8 *F*, *red line*). This implies that the trimeric form of SS-EGFP-SUN2$^{261–731}$ associates with the nuclear membrane and thus diffuses slowly. Because SUN2 oligomerization is required for KASH-binding (18), it is possible that this membrane association is mediated by interaction of SS-EGFP-SUN2$^{261–731}$ with the KASH peptides of endogenous nesprin proteins present at the ONM. Relatedly, the increase of the fast diffusing component as b decreases, suggests that monomeric SS-EGFP-SUN2$^{261–731}$ diffuses through the PNS.

The MSQ analysis of SS-EGFP-SUN2$^{261–731}$ was performed without accounting for the exponential correlation process. This is justified, because at high N, where the volume fluctuations at the NE are most easy to observe, the brightness is close to three. Under these conditions, SS-EGFP-SUN2$^{261–731}$ is associated with the membrane, and therefore the fluorescence of the sample is not affected by the distance fluctuations of the nuclear membranes.

CONCLUSIONS

This study describes the unique challenges for FFS and brightness analysis when quantifying protein oligomerization in the NE. We discovered the existence, to our knowledge, of a novel intensity fluctuation process in the NE, which renders conventional brightness analysis of FFS data in this subcellular compartment unreliable. Furthermore, we provided evidence to suggest that nanometer fluctuations in the separation of the INM and ONM are the cause of this process. The experimental data revealed that an exponential correlation term was sufficient to model the PNS volume fluctuations with an amplitude that was approximately proportional to fluorescence intensity. The incorporation of this exponential correlation term into MSQ analysis enabled the calculation of the oligomeric state and diffusion time for EGFP-tagged luminal proteins. We further recognized that the correlation time of the PNS volume fluctuations was sufficiently slow to lead to discrepancies between ACF and MSQ analysis, which originated from the fixed segment period used for calculating the ACF. To correct for these inconsistencies, we introduced a correlation term (Eq. 9) that accounts for the finite segment time, and thereby allows for future analysis of FFS data taken in the NE not only by MSQ but also by ACF analysis. Finally, we demonstrated the ability of MSQ analysis to identify the oligomeric state of EGFP-tagged NE protein constructs encoding the KASH peptide of nesprin-2 or the luminal domain of SUN2. The brightness of the luminal SUN2 construct increased from a monomer to approximately a trimer, which agrees with results obtained in vitro (27).

In summary, this work lays the foundation for future quantitative characterization of protein oligomerization in the NE by FFS and brightness analysis. Future efforts are needed to fully characterize the nature of the distance fluctuations between the nuclear membranes and their influence on FFS experiments. Whereas the presence of these fluctuations complicates the interpretation of FFS data collected in the NE, they also provide a means for distinguishing between NE proteins that are freely diffusing through the PNS and proteins that are associated with the nuclear membranes.

SUPPORTING MATERIAL

Supporting Materials and Methods and one table are available at http://www.biophysj.org/biophysj/supplemental/S0006-3495(17)30613-6.

AUTHOR CONTRIBUTIONS

J.H. designed and performed research, analyzed data, and wrote the manuscript. K.-H.H. contributed analytical tools and wrote the manuscript. C.A.S. designed research and constructed plasmids. G.W.G.L. designed research and wrote the manuscript. J.D.M. designed research, analyzed data, and wrote the manuscript.

ACKNOWLEDGMENTS

This research was supported by the National Institutes of Health (NIH) (GM064589 to J.D.M. and AR007612 to C.A.S.) and the Dystonia Medical Research Foundation (to G.W.G.L. and J.D.M.).

REFERENCES

1. Watson, M. L. 1955. The nuclear envelope; its structure and relation to cytoplasmic membranes. *J. Biophys. Biochem. Cytol.* 1:257–270.
2. Wente, S. R., and M. P. Rout. 2010. The nuclear pore complex and nuclear transport. *Cold Spring Harb. Perspect. Biol.* 2:a000562.
3. Dauer, W. T., and H. J. Worman. 2009. The nuclear envelope as a signaling node in development and disease. *Dev. Cell.* 17:626–638.
4. Wilson, K. L., and J. M. Berk. 2010. The nuclear envelope at a glance. *J. Cell Sci.* 123:1973–1978.
5. Worman, H. J., and W. T. Dauer. 2014. The nuclear envelope: an intriguing focal point for neurogenetic disease. *Neurotherapeutics.* 11:764–772.
6. Kask, P., K. Palo, …, K. Gall. 1999. Fluorescence-intensity distribution analysis and its application in biomolecular detection technology. *Proc. Natl. Acad. Sci. USA.* 96:13756–13761.
7. Chen, Y., J. D. Müller, …, E. Gratton. 1999. The photon counting histogram in fluorescence fluctuation spectroscopy. *Biophys. J.* 77:553–567.
8. Chen, Y., and J. D. Müller. 2007. Determining the stoichiometry of protein heterocomplexes in living cells with fluorescence fluctuation spectroscopy. *Proc. Natl. Acad. Sci. USA.* 104:3147–3152.
9. Jameson, D. M., J. A. Ross, and J. P. Albanesi. 2009. Fluorescence fluctuation spectroscopy: ushering in a new age of enlightenment for cellular dynamics. *Biophys. Rev.* 1:105–118.

10. Wu, B., J. A. Chao, and R. H. Singer. 2012. Fluorescence fluctuation spectroscopy enables quantitative imaging of single mRNAs in living cells. *Biophys. J.* 102:2936–2944.
11. James, N. G., M. A. Digman, …, D. M. Jameson. 2012. Number and brightness analysis of LRRK2 oligomerization in live cells. *Biophys. J.* 102:L41–L43.
12. Smith, E. M., P. J. MacDonald, …, J. D. Mueller. 2014. Quantifying protein-protein interactions of peripheral membrane proteins by fluorescence brightness analysis. *Biophys. J.* 107:66–75.
13. Hur, K.-H., and J. D. Mueller. 2015. Quantitative brightness analysis of fluorescence intensity fluctuations in *E. coli*. *PLoS One.* 10:e0130063.
14. Crisp, M., Q. Liu, …, D. Hodzic. 2006. Coupling of the nucleus and cytoplasm: role of the LINC complex. *J. Cell Biol.* 172:41–53.
15. Chang, W., H. J. Worman, and G. G. Gundersen. 2015. Accessorizing and anchoring the LINC complex for multifunctionality. *J. Cell Biol.* 208:11–22.
16. Gundersen, G. G., and H. J. Worman. 2013. Nuclear positioning. *Cell.* 152:1376–1389.
17. Wang, N., J. D. Tytell, and D. E. Ingber. 2009. Mechanotransduction at a distance: mechanically coupling the extracellular matrix with the nucleus. *Nat. Rev. Mol. Cell Biol.* 10:75–82.
18. Sosa, B. A., A. Rothballer, …, T. U. Schwartz. 2012. LINC complexes form by binding of three KASH peptides to domain interfaces of trimeric SUN proteins. *Cell.* 149:1035–1047.
19. Smith, E. M., J. Hennen, …, J. D. Mueller. 2015. In situ quantification of protein binding to the plasma membrane. *Biophys. J.* 108:2648–2657.
20. MacDonald, P. J., Y. Chen, …, J. D. Mueller. 2010. Brightness analysis by Z-scan fluorescence fluctuation spectroscopy for the study of protein interactions within living cells. *Biophys. J.* 99:979–988.
21. Sanchez-Andres, A., Y. Chen, and J. D. Müller. 2005. Molecular brightness determined from a generalized form of Mandel's Q-parameter. *Biophys. J.* 89:3531–3547.
22. Mandel, L. 1979. Sub-Poissonian photon statistics in resonance fluorescence. *Opt. Lett.* 4:205–207.
23. Chen, Y., L.-N. Wei, and J. D. Müller. 2003. Probing protein oligomerization in living cells with fluorescence fluctuation spectroscopy. *Proc. Natl. Acad. Sci. USA.* 100:15492–15497.
24. Müller, J. D. 2004. Cumulant analysis in fluorescence fluctuation spectroscopy. *Biophys. J.* 86:3981–3992.
25. Wu, B., and J. D. Müller. 2005. Time-integrated fluorescence cumulant analysis in fluorescence fluctuation spectroscopy. *Biophys. J.* 89:2721–2735.
26. Hur, K.-H., P. J. MacDonald, …, J. D. Mueller. 2014. Quantitative measurement of brightness from living cells in the presence of photodepletion. *PLoS One.* 9:e97440.
27. Goodchild, R. E., and W. T. Dauer. 2004. Mislocalization to the nuclear envelope: an effect of the dystonia-causing torsinA mutation. *Proc. Natl. Acad. Sci. USA.* 101:847–852.
28. Chen, Y., J. D. Müller, …, E. Gratton. 2002. Molecular brightness characterization of EGFP in vivo by fluorescence fluctuation spectroscopy. *Biophys. J.* 82:133–144.
29. Seifert, U. 1997. Configurations of fluid membranes and vesicles. *Adv. Phys.* 46:13–137.
30. Vander Heyden, A. B., T. V. Naismith, …, P. I. Hanson. 2011. Static retention of the lumenal monotopic membrane protein torsinA in the endoplasmic reticulum. *EMBO J.* 30:3217–3231.
31. Ostlund, C., E. S. Folker, …, H. J. Worman. 2009. Dynamics and molecular interactions of linker of nucleoskeleton and cytoskeleton (LINC) complex proteins. *J. Cell Sci.* 122:4099–4108.